International Journal of Nanomedicine

Dovepress
Taylor & Francis Group

Open Access Full Text Article

ORIGINAL RESEARCH

Golden Tandem of Photothermal Ablation and Simultaneous Anti-Inflammation in One Nanoparticle for Activated Macrophage-Targeted Atherosclerosis Treatment

Yuqing Lu[1,*], Yan Wang[2,*], Yize Li[1,*], Yunan Li[1], Yao-Wen Jiang[1,3], Jingjing Li[1,3]

[1]School of Medical Imaging, Xuzhou Medical University, Xuzhou, 221004, People's Republic of China; [2]The First Clinical Medical College, Xuzhou Medical University, Xuzhou, 221004, People's Republic of China; [3]Department of Radiology, Affiliated Hospital of Xuzhou Medical University, Xuzhou, 221006, People's Republic of China

*These authors contributed equally to this work

Correspondence: Yao-Wen Jiang; Jingjing Li, Email jiang@xzhmu.edu.cn; qingchao0124@163.com

Introduction: Photothermal therapy (PTT) is attracting increasing attention in treating atherosclerotic plaques. However, PTT can induce inflammatory responses, in turn stimulating the regeneration of atherosclerosis and hindering subsequent therapy.

Methods: In this paper, a multifunctional nanoparticle (Au NR@SiO_2/RSNO/DS, GSNPD) for the synergistic treatment of atherosclerosis through PTT and anti-inflammation effects was developed. The preparation and characterization of GSNPD, their cellular toxicity, photothermal conversion and targeted ablation efficiency, anti-inflammation and ROS scavenging effect, as well as the inhibition of foam cell formation were studied in vitro.

Results: The experimental results showed that the fabricated GSNPD NPs displayed positive effects on anti-atherosclerosis by pro-inflammatory macrophages ablation, NO production and ROS scavenging.

Discussion: GSNPD NPs were designed to effectively and accurately ablate pro-inflammatory macrophages by recognizing and targeting to SR-A overexpressed on the activated macrophages of arterial plaques via PTT, and simultaneous inhibit the PTT-induced inflammation through the laser-activated NO release in situ. This match of therapeutic agents and inhibitors not only achieves good therapeutic effects but also minimizes side effects as much as possible, which may provide an effective way for PTT-based treatment of atherosclerosis.

Keywords: gold nanorods, photothermal therapy, NO, activated macrophages, atherosclerosis

Introduction

Atherosclerosis (AS) is a complex chronic inflammatory process leading to cardiovascular disease (CVD), a disease caused by the increased blood cholesterol carried in low-density lipoprotein (LDL).[1] Deposits of lipids and fibrous components under the walls of large arteries can affect large- and medium-sized arteries, inducing the formation of atherosclerotic plaques. Atherosclerosis is a primary contributor to vascular disease around the world.[2,3] Thus, early intervention and prevention are essential for atherosclerotic plaque progression.[4] Surgical treatment is an invasive treatment that can induce acute cardiovascular events and is risky. Dissection and occlusion of the internal carotid artery can occur during or following carotid endarterectomy.[5] Furthermore, clinical oral drugs such as statins and testosterone to decrease lipid levels can provide effective treatment, but traditional oral drugs are always limited by poor targeting ability and long periods before acting, which would result in various adverse side effects.[6,7] Therefore, a noninvasive and effective treatment tactic is urgently needed to inhibit the progression of early atherosclerotic plaque.

Received: 20 November 2024
Accepted: 30 January 2025
Published: 7 February 2025

PTT is a therapeutic modality that realizes hyperthermia in specific regions by converting light energy into thermal energy. The core principle of PTT is the utilization of the photothermal effect (PTE) of photothermal transduction agents (PTAs), such as photosensitizers or nanoparticles.[8] These materials will promptly transform the absorbed light of specific wavelengths into thermal energy, resulting in a local temperature increase. The increase in temperature usually reaches 42 ~ 45°C, which is sufficient to induce apoptosis or necrosis of cells without affecting the surrounding normal tissues. PTT is an emerging cancer treatment technology and has also received certain research in atherosclerosis.[9–11] In recent years, numerous studies have indicated that it is a highly effective therapeutic approach for reducing atherosclerotic plaque, owing to the advantages of flexibility, minimal invasion and high spatial precision.[12] PTT can ablate macrophages and reduce lesions to improve the plaque micro-environment.[13,14] Nevertheless, PTT still has several shortcomings and challenges to overcome. For example, the tissue penetration depth of near-infrared light (NIR) is restricted, typically reaching only a few centimeters, which limits the therapeutic efficacy of PTT on deep tissues. Additionally, as a result of the thermal diffusion effect, the surrounding normal tissues might undergo thermal injury. What's more, the inflammatory effects brought by PTT should also be taken seriously. Controlling the scope and extent of local temperature increase poses a challenge. However, the introduction of nanoparticles can solve some of the problems. Nanoparticles serving as PTAs (such as gold nanorods, graphene, carbon nanotubes, etc.) have a higher photothermal efficiency than molecular PTAs.[15] With the advancement of nanotechnology, various metal photothermal conversion nanoparticles have garnered growing interest due to their robust light absorption and transformation capabilities attributed to the surface plasmon resonance (SPR) effect. Such as, Ag@S-nitrosothiol nanoparticles, Cu_3BiS_3 nanocrystals, and $CuCo_2S_4$ nanocrystals have been used in PTT for atherosclerosis.[16–18] Furthermore, nanoparticle PTAs can combine targeting ability with multiple imaging modalities and therapeutic functions, presenting unique advantages.[19]

Macrophage proliferation accumulation plays a key role in atherosclerosis.[20,21] Pro-inflammatory (M1-like) phenotype can highly release inflammatory cytokines (TNF-α, IL-6) and generate a good deal of reactive oxygen species (ROS). However, pro-resolving (M2-like) phenotypes can dampen inflammation. Macrophage class-A scavenger receptors (SR-A) are involved in the pathological accumulation of cholesterol in atherosclerosis. The macrophages in atherosclerotic lesions presented the classical 'foamy' appearance due to macrophage scavenger receptors mediated the uptake of oxidized cholesterol.[22,23] Thus, macrophages are commonly treated as an effective target for PTT ablation to inhibit atherosclerosis progression.[11,24] However, an unavoidable issue for PTT-based atherosclerosis treatment is the accompanying side effect, inflammatory responses, which will weaken treatment effectiveness. Thus, the synergistic therapy of PTT and anti-inflammatory might be a helpful strategy.

To achieve this objective, in this work, we utilized silica-encapsulated gold nanorods ($Au@SiO_2$) as PTT agents and nanocarriers. After conjugation with the heat-sensitive RSNO molecules to release NO in situ as anti-inflammatory agent, DS was further modified to serve as a molecular targeting ligand for SR-A, which is overexpressed in inflammatory macrophages.[25] The obtained nanoparticles (GSNPD) can not only target and ablate inflammatory macrophages but also relieve inflammation by heat-controlled NO release (Scheme 1). It has been reported that a deficiency in the production or activity of NO may contribute to the development of atherosclerosis.[26] As a cell signaling molecule, it is well known that NO can regulate vascular tension.[27] NO can weaken the inflammatory response and inhibit the progression of plaques at the lesion sites.[28] DS is a hydrophilic and negatively charged polysaccharide, featuring excellent biodegradability and biocompatibility.[25] DS can selectively combine with the positively charged residues of SR-A through ligand-receptor recognition.[29] Previous studies have probed into the application of various DS-coated nanomaterials in atherosclerotic plaque imaging, with the aim of targeting activated macrophages.[30] DS as a targeting molecule also confers the benefit of stabilizing and attenuating atherosclerotic plaques, as it competitively inhibits the internalization of oxidized low-density lipoproteins (ox-LDLs) via SR-A occupancy.[31] In our research, DS was employed as the preferred ligand for SR-A on activated macrophages to enhance the targeting and penetration capabilities of nanoparticles. As expected, such GSNPD NPs exhibited high photothermal properties and controllable NO generation to inhibit macrophage foaming and improve the inflammatory micro-environment in vitro.

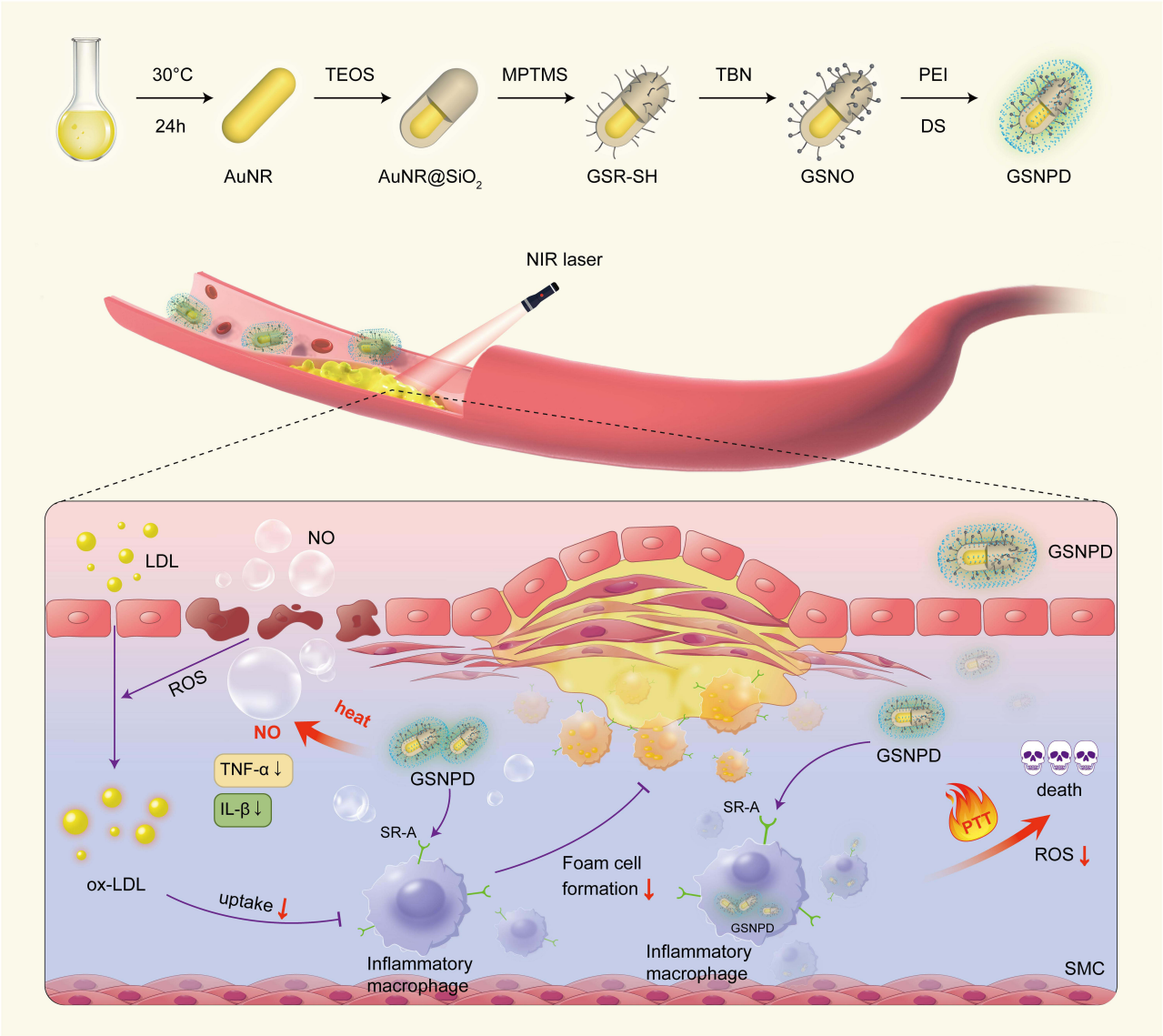

Scheme 1 The schematic diagram of GSNPD NP preparation and its photothermal/anti-inflammatory therapy for atherosclerosis.

Methods

Materials

Hexadecyltrimethylammonium bromide (CTAB) was obtained from Wigedbio Technology Co., Ltd. (Xuzhou, China). Tetrachloroauric acid trihydrate 99.5% ($HAuCl_4 \cdot 3H_2O$) was acquired from ACMEC Biochemical Technology Co., Ltd. (Shanghai, China). Silver nitrate ($AgNO_3$, 99%), Sodium borohydride ($NaBH_4$, 96%) L-Ascorbic acid (L-AA, 99.7%), Hydrochloric acid, tetraethyl orthosilicate (TEOS), ethanol, and methanol were bought from SinopharmChemReagent Co., Ltd. (Shanghai, China). Dextran sulfate (DS) was obtained from Yuanye Bio-Technology Co., Ltd. (Shanghai, China). Sodium hydroxide (NaOH, 96%), 3-(mercaptopropyl) trimethoxysilane (MPTMS, 97%), Rhodamine 6G (Rh6G), tert-Butyl nitrite (TBN, 90%) were obtained from Macklin Biochemical Technology Co., Ltd. (Shanghai, China). Nitrate Assay Kit, BODIPY 493/503 Staining Kit and Lipopolysaccharides (LPS) were gained from Beyotime Biotechnology Co., Ltd. (Shanghai, China). The CCK-8 cell counting kit, phosphate buffer saline (PBS), and Calcein AM/PI reagents were obtained from Meilun Biotechnology Co., Ltd. (Dalian, China). Fetal bovine serum (FBS), penicillin–streptomycin and Dulbecco's modified eagle medium (DMEM) were obtained from Gibco (USA). Four percent paraformaldehyde was obtained

https://doi.org/10.2147/IJN.S503774

from Saiguo Biotech Co., Ltd. (Guangzhou, China). Enzyme-linked immunosorbent assay (ELISA kits) was provided by Jianglaibio Technology Co., Ltd. (Shanghai, China). The Oil red O(ORO) staining kit and oxidized low-density lipoprotein (ox-LDL) were provided by Solarbio Science & Technology Co., Ltd. (Beijing, China). Balb/c mice (8 week) were provided by the Animal Center of Xuzhou Medical University. All animal experiments were approved by the Animal Care Committee of Xuzhou Medical University (approval number: 202307T031). All animal experiments were conducted according to the guidelines of the National Institutes of Health on the use of animals in research.

Preparation of Au NR@SiO_2 (GSR)

The gold nanorods were synthesized using a seed-mediated growth method with minor modifications.[32] Firstly, we mixed 2.5 mL of CTAB (0.1 M) solution and 83 μL of $HAuCl_4$ (10 mM) aqueous solution. After that, 0.2 mL of iced $NaBH_4$ (0.01 M) was slowly added and stirred continuously. Subsequently, the solution was incubated in a 25 °C water bath for 2 h. Secondly, 4.8 mL of $HAuCl_4$ (0.01 M) solution was added to 114 mL of CTAB (0.1 M) solution, succeeded by the sequential addition of 720 μL of $AgNO_3$ (0.01 M) aqueous solution, 40 μL of 36.5% HCl and 768 μL of L-ascorbic acid (0.1 M) solution. Finally, 240 μL of the gold seed solution was added, and the mixture was incubated overnight at 30 °C. The obtained 30 mL aliquot of GNR solution was centrifuged (18000 rpm, 15 min) once and dispersed. Then, 60 μL of 20% TEOS methanol solution was mixed with 15 mL of GNR aqueous solution for three times at 30-minutes intervals (pH 10–11). The mixture reacted for two days at 26 ~28 °C.

Preparation of Au NR@SiO_2-SNO (GSNO)

To modify -SH groups on the surface of SiO_2 shells, firstly, 300 μL of MPTMS was added to 15 mL of GNR@SiO_2 aqueous solution and transferred the mixture to an oil bath with the temperature rising to 90 °C. After four hours reflow, the GNR@SiO_2-SH nanorods (GSN) were washed twice and re-dispersed in methanol for later use. To turn -SH groups into -SNO groups, we added an excess of t-butyl nitrite (~400 μL). The mixture was quickly stirred overnight in the dark at room temperature. The final product, GNR@SiO_2-SNO (GSNO), was washed twice successively with water and methanol, then dispersed and stored for subsequent use.

Preparation of Au NR@SiO_2-SNO-PEI/DS (GSNPD)

Two milliliters of PEI (2 mg/mL) solution was added to 2 mL of GSNO (1 mg/mL) solution, and stirred rapidly for 4 h. Subsequently, the mixture was washed and centrifuged (14000 rpm, 30 min) three times. GSNPDs were prepared by electrostatic adsorption.[33] In a word, 1 mL of DS (10 mg/mL) was mixed with 1 mL of GSNP (1 mg/mL) solution and stirred continuously on an iced rocker. Finally, the precipitate was washed three times to obtain Au NR@SiO_2-SNO-PEI /DS (GSNPD) NPs.

Characterization of Au NR@SiO_2-SNO-PEI/DS (GSNPD)

Transmission electron microscopy (TEM) (FEI Tecnai G2 F30) was used to detect the morphology and size of the GSNPD NPs. The characteristic spectra were characterized by UV-vis spectrophotometer and Fourier infrared spectrometer, respectively. Zetasizer was utilized to measure zeta potential, while dynamic light scattering (DLS) was employed to evaluate potential variations, particle size, and distribution stability. The elemental composition of the GSNO was measured by a high-resolution TEM (FEI Tecnai G2 F30). Thermal images were captured using a thermal imaging camera. An 808 nm laser was applied to induce photothermal effects.

Photothermal Experiments

The photothermal performance of GSNPD NPs was detected with an infrared thermal camera. Primarily, 808 nm laser (2 W/cm^2, 5 min) was applied to irradiate various concentrations (0, 12.5, 25, 50, 100, 200, 400 μg/mL) of GSNPD NPs solution and the temperatures of GSNPD NPs solution were monitored by infrared thermography at an interval of 30s. Similarly, the GSNPD NPs solution (200 μg/mL) was exposed to a 808 nm laser at various

power densities (1, 1.5, 2, and 4 W/cm^2) last 5 min. To evaluate the photothermal conversion efficiency (η) of GSNPD NPs, the temperature was recorded at the set time until the temperature inclined to be stable. Later, we turned off the laser and then cooled to room temperature. According to the formula[34] below, the photothermal conversion efficiency (η) was measured:

$$\eta = \frac{hs\,(T_{\max} - T_{surr}) - Q_{dis}}{I\,(1 - 10^{-A808})}$$

To assess the photothermal stability, a 808 nm laser (2 W/cm^2) was employed to irradiate GSNPD NPs solution for 5 min. Subsequently, the temperature of GSNPD NPs solution returned to room temperature after turning off the laser. The ON/OFF cycle irradiation experiment of GSNPD NPs solution was conducted for 4 cycles.

Measurement of NO Release from GSNPD Nanoparticles in Aqueous Solution

To quantify the NO release from the GSNPD NPs solution, a standard Griess assay was employed. When NO is released from NPs, it will immediately react with the Griess reagent, turning the solution pink.[35] The absorption signal of the GSNPD NPs solution was measured, and the concentration of NO in the solution was calculated using a $NaNO_2$ standard curve.

Cell Culture

Mouse macrophage cells (RAW264.7 cell line) were purchased from Fuheng biology (Shanghai, China). Cells were cultured in high-glucose Dulbecco's Modified Eagle's Medium (DMEM) supplemented with 1% penicillin/streptomycin and 10% fetal bovine serum at 37°C under 5% CO_2. RAW264.7 cells were activated with 1 μg/mL lipopolysaccharide (LPS) overnight. To induce foam cell formation, RAW264.7 cells were incubated with 60 μg/mL ox-LDL solution prepared in DMEM medium containing 5% FBS for 48 hours.

Cell Cytotoxicity Evaluation and Hemolysis Test

Cytotoxicity analysis was assessed by the CCK-8 assay. In brief, RAW264.7 cells were cultured and incubated overnight. Then, 100 μL of culture medium including various concentrations of GSNPD NPs (0, 6.25, 12.5, 25, 50, 100, 200, 300 μg/mL) was added. After being incubated overnight, cells were washed and incubated for 2 h after the addition of 100 μL of fresh medium and 10 μL of CCK-8 reagent. We detected the absorbance of the medium at 450 nm and calculated the mean absorbance (OD) of three wells in each group:

$$\text{cell viability } (\%) = \frac{OD\,(treatment\ group) - OD\,(blank)}{OD\,(control) - OD\,(blank)} \times 100\%$$

Fresh mouse blood was obtained for the hemolysis experiment. Firstly, 200 μL of RBC solution was mixed with 800 μL of GSNPD NPs with different concentrations (25, 50, 100, 200, and 400 μg/mL) and incubated for two hours. Secondly, RBCs were treated with an equivalent volume of deionized water and saline as the positive and negative controls, respectively. Finally, the cells were centrifuged and the absorbance of the supernatant was measured at 541 nm. The results of the hemolysis experiment were calculated as follows:

$$\text{Hemolysis } (\%) = \frac{OD\,(sample) - OD\,(negative\ control)}{OD\,(positive\ control) - OD\,(negative\ control\ group)} \times 100\%$$

In vitro Targeting Ability

Rhodamine 6G (Rh 6G)-labeled nanoparticles were used to trace the intracellular distribution of GSNO and GSNPD NPs. For subsequent experiments, RAW264.7 cells were cultured and incubated with LPS overnight. Afterwards, we sucked out the medium and added 500 μL of medium containing Rh-6G labeled GSNPD NPs (200 μg/mL). The medium was aspirated and washed at different times (10, 20, 30, 60, 120 min). Following this, the cells that had underwent phagocytosis of materials were fixed in 4% paraformaldehyde and stained with DAPI prior to observation. To evaluate

the ability of DS in targeting inflammatory macrophages, cells were primarily co-incubated with LPS (1 μg/mL) stimulation overnight. Afterwards, the cells were incubated with Rh-6G labelled GSNO or GSNPD NPs (200 μg/mL), respectively. Besides, the cells were washed and stained after 30 min of incubation. Fluorescence images were subsequently obtained using confocal laser scanning microscopy at 405 nm and 514 nm excitation. Flow cytometry was utilized to quantify the intracellular signal of RAW264.7 cells after different treatments. The intracellular Au in RAW264.7 cells following various treatments was quantified using inductively coupled plasma mass spectrometry (ICP-MS).

RAW264.7 cells were cultured with or without LPS stimulation overnight to investigate the influence of NPs on ox-LDL uptake by macrophages. Subsequently, either GSNO or GSNPD NPs (200 μg/mL) were added, respectively. Following this, 60 μg/mL of ox-LDL was added for four hours incubation after removing the remaining materials. Confocal laser scanning microscopy was applied to obtain the fluorescence images at 405 nm and 514 nm excitation after the cells were washed and stained with Hoechst 33342 and BODIPY 493/503 for 15 min.

In vitro PTT Effect

GSNPD NPs containing different concentrations (0–200 μg/mL) were used to replace the medium after the cells were inoculated and incubated with LPS (1 μg/mL) overnight. Following, the cells were treated with or without a 808 nm (2 W/cm^2) irradiation laser for 5 min after removing the surplus NPs. To assess the cell viability at different concentrations, the absorbance of the medium was measured after adding 10 μL of CCK-8 solution. Besides, the cell viability of activated macrophages with various treatments (control, laser, GSNO, GSNPD, GSNO + laser, and GSNPD + laser) was detected in the same way. To confirm the influence of GSNPD+laser on normal macrophages, macrophages without LPS treatment were performed as control.

The PTT effect was assessed by live/dead cell co-staining assay. In this study, the activated macrophages with the above treatment were incubated with Calcein-AM/PI in the dark. After being washed, the cells in a 6-well plate were imaged under a fluorescent inverted microscope.

Cell Apoptosis Analysis

RAW264.7 cells in all groups, except for control group, were pre-treated with LPS before being subjected to various treatments (control, laser, GSNO, GSNPD, GSNO + laser, and GSNPD + laser). After 12 hours, the cells were collected and re-suspended in 500 μL of PBS, followed by staining with Annexin V-FITC and PI at room temperature. Finally, apoptosis analysis was performed using flow cytometry to evaluate the effects of different treatments.

Inhibit the Generation of Reactive Oxygen Species (ROS)

RAW264.7 cells in all groups except the control group were LPS pre-treated before the cells were treated with various treatments (control, LPS, GSNO, GSNPD, GSNO + laser, and GSNPD + laser). After 12 h, the fresh medium containing DCFH-DA replaced the cell culture mediums and incubated for an additional 30 min. The intracellular ROS generation in different treatments could be observed using a fluorescence-inverted microscope after washing. To show the influence of GSNPD + laser on ROS production from normal macrophages, macrophages without LPS treatment were performed as control.

Anti-Inflammation Performance of GSNPD NPs

The influence of GSNPD NPs on the secretion of inflammation factors in RAW264.7 cells was evaluated using an ELISA assay. Cells were subjected to different treatments (control, LPS, laser, GSPD + laser, GSNO + laser, and GSNPD + laser) overnight, and the concentration of pro-inflammatory factors (TNF-α, IL-6) in the supernatant were measured using an ELISA kit.

Foam Cell Formation Assay

0.4 μm pore Transwell chambers (LABSELECT) with polycarbonate filters were used for foam cell formation assay. Activated macrophages were seeded in the upper chamber, while unactivated macrophages were seeded in the bottom chamber simultaneously. The cells in the upper chamber were subjected to different treatments (control, LPS, laser, GSPD + laser, GSNO + laser, and GSNPD + laser) for four hours. Subsequently, the medium was replaced, and the cells

were further incubated overnight. After that, 60 μg/mL ox-LDL was introduced into the bottom chamber and incubated for two days. The lipid droplet generation was observed by a fluorescence microscope in a bright field.

Statistical Analysis

The data were analyzed using the GraphPad Prism software. A *T*-test (nonparametric tests) was applied for mean comparisons, and data were reported as mean ± SD. *p < 0.05, **p < 0.01, ***p < 0.001 and ****P < 0.0001 were used to indicate the significance of the difference.

Results

Synthesis and Characterization of GSNPD

To obtain GSNPD NPs, the seed-mediated growth method was used to prepare GNR. Then, using the modified Stöber method, a uniform silica shell was encapsulated on the surface of GNR to form AuNR@SiO_2 (GSR). In addition, the elemental composition of GNR was enriched to facilitate subsequent surface sulfhydryl modification and nitrothiol loading. After thiolation, GSNO was obtained by the conversion of SH to SNO. Finally, DS was modified with the help of PEI through electrostatic adsorption. The morphology of the GNR, GSR, GSNO, and GSNPD NPs was detected by transmission electron microscopy (TEM) (Figure 1A), which indicated that GNRs had an average length of 33.3 ± 6.3 nm and an average width of 11.7 ± 1.7 nm. By comparing the TEM images of GSN and GSR, a uniform silica shell with a thickness of ~15 nm was grown on GNR obviously, indicating the successful forming of GSR as expected via the hydrolysis of TEOS (Figure 1A). Importantly, the original morphology of the GNR remained unchanged during the coating process, indicating that the silica shell was deposited without causing any deformation. The high-resolution TEM further validated the elemental composition (Au, Si, O, S, and N) of GSNO (Figure S1), indicating that GNR were encapsulated within the silica shell. Moreover, uniform distribution of these elements throughout the structure of GSNO confirms the consistency of the coating process. The UV-vis absorption spectra (Figure 1B) showed that GNR had

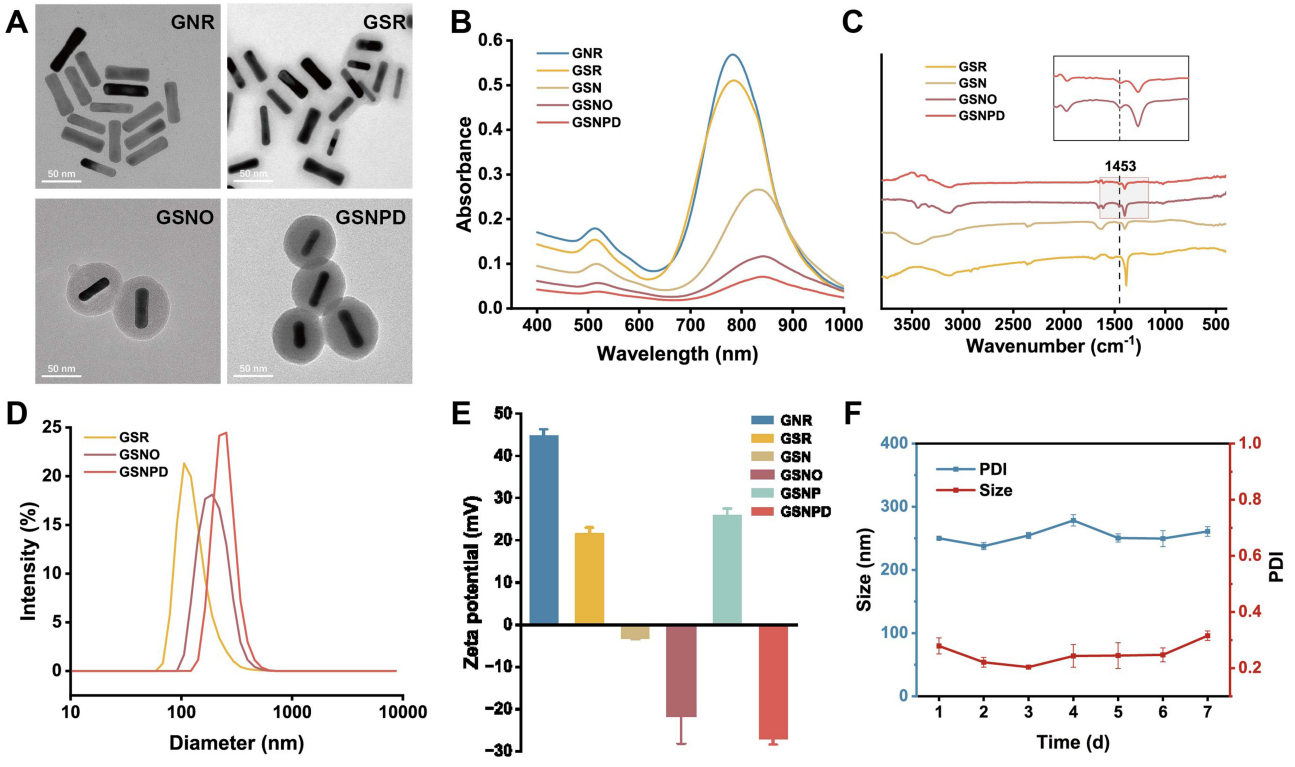

Figure 1 (**A**) TEM images of GNR, GSR, GSNO, and GSNPD. (**B**) UV-vis absorption spectra of GNR, GSR, GSN, GSNO, and GSNPD. (**C**) FTIR spectra of GSR, GSN, GSNO and GSNPD. Inset: enlarged FTIR spectra of 1453 cm^{-1} from 1600–1300 cm^{-1}. (**D**) Hydrodynamic diameters of GSR, GSNO, and GSNPD. (**E**) Zeta potentials of GNR, GSR, GSN, GSNO, GSNP, and GSNPD (n = 3). (**F**) Hydrodynamic size changes of GSNPD as a function of time (n = 3).

https://doi.org/10.2147/IJN.S503774

a longitudinal localized surface plasmon resonance (LSPR) at 790 nm. After subsequent modification, LSPR exhibited successive red shifts within the optimal NIR absorption window for photothermal application. Furthermore, the Fourier transform infrared spectroscopy (FTIR) spectrum of GSNO showed an emerging characteristic peak of -N=O at 1453 cm^{-1} (Figure 1C), which verified the successful conjugation of -SNO onto GSR. We obtained the average hydrodynamic diameters of GSR, GSNO, and GSNPD via dynamic light scattering (DLS). The sizes were around 106 nm, 190 nm, and 255 nm, respectively (Figure 1D). After each step of successful assembly, the hydrodynamic diameters enlarged correspondingly. The size of GSR, GSNO, and GSNPD NPs measured by DLS was generally more extensive than that observed by TEM due to the fact that DLS measures the radius of hydrated particles. Besides, the zeta potential shifted from +44.8 mV for GNR to −27.1 mV for GSNPD (Figure 1E), which further confirmed the successful preparation of GSNPD NPs. After silica coating, the zeta potential decreased from +44.8 mV (GNR) to +21.6 mV (GSR). Subsequently, the zeta potentials showed significant charge reversal from +21.6 mV (GSR) to −3.2 mV (GSN) due to the abundance of -SH groups, and the effective loading of TBN further lowered GSNO to be −21.6 mV. Since PEI is positively charged, the zeta potential of GSNP increased to +25.8 mV after PEI covering. Finally, DS was added by electrostatic adsorption, and the zeta potential of GSNPD decreased to −27.1 mV. The above results proved the successful preparation of GSNPD. More importantly, GSNPD NPs had negligible changes in hydrodynamic size within a week, indicating the superior stability of GSNPD NPs in a physiological environment (Figure 1F).

Photothermal Conversion Efficiency

The UV-vis absorption spectrum of GSNPD NPs exhibited intense and broad absorption in the range from 500 to 900 nm, indicating that GSNPD NPs are excellent photothermal agent. Thermal imaging was employed to monitor the temperature of the GSNPD solution under an 808 nm laser (2 W/cm^2) at various concentrations and power intensities (Figure 2A and B). To evaluate the photothermal conversion performance of GSNPD NPs, aqueous suspensions of GSNPD NPs were irradiated at elevated concentrations (0, 25, 50, 100, 200, 400 μg/mL) under an 808 nm laser (2 W/cm^2) or power densities (0.5, 1.0, 1.5, 2.0, 4.0 W/cm^2 at 200 μg/mL). The photothermal heating curve of GSNPD aqueous solution indicated that the increase in temperature depended on the concentration of GSNPD NPs, irradiation time and power intensity of the 808 nm laser (Figure 2C and D). Especially with the concentration of GSNPD NPs at 200 μg/mL, the increase in temperature could reach 23°C in 6 min of irradiation (2 W/cm^2), which is sufficient to induce cell apoptosis. No discernible temperature change was observed when deionized water was exposed to the laser at the same power density, indicating that the presence of GSNPD NPs enabled efficient and rapid conversion of 808 nm irradiation into thermal energy. As demonstrated in Figure 2E, the similar temperature in each cycle confirmed the outstanding photo-stability of GSNPD NPs, highlighting the potential of the composite nanoparticles to function as an effective photothermal agent for subsequent NO generation and PTT of atherosclerosis. To further determine the NIR photothermal conversion efficiency (PCE, η), a 808 nm laser (2 W/cm^2) was used to irradiate GSNPD NPs aqueous solution (200 μg/mL) for 15 min. The PCE was calculated to be 68.77% (Figure S2), which provided a basis for the following synergistic therapy of PTT and anti-inflammation of atherosclerosis.

Measurement of NO Release from GSNPD NPs

The multifunctional GSNPD NPs can be used as a promising NIR-activated NO-releasing platform. NO release from S-nitroso thiols was realized by homolytic cleavage of the S-N bond under light or heat.[36] In this study, a classical Griess assay was used to confirm and quantify the NO release and the standard curve was first detected (Figure S3). As shown in Figure 2F, the NIR laser triggered GSNPD NPs to release NO, and as the laser power density increased, both the amount and rate of NO-releasing increased, indicating the density-dependent features of NO release. Furthermore, the designed GSNPD NPs displayed high stability at a physiological temperature of 37 °C and did not release NO gas unless irradiated with a 808 nm laser (2W/cm^2), illustrating specific NIR-controlled NO generation (Figure 2G). To further investigate such controllable NO gas-releasing behavior of GSNPD NPs, intermittent laser irradiation was adopted. As demonstrated in Figure 2H, with continuous irradiation for 10 min, GSNPD NPs produced a large amount of NO gas, and the generation rate increased with prolonged irradiation time. The NO gas generating rate was significantly reduced after turning off the laser for 10 min. Given that GSNPD NPs would generate NO rapidly over 45 °C, we adjusted the

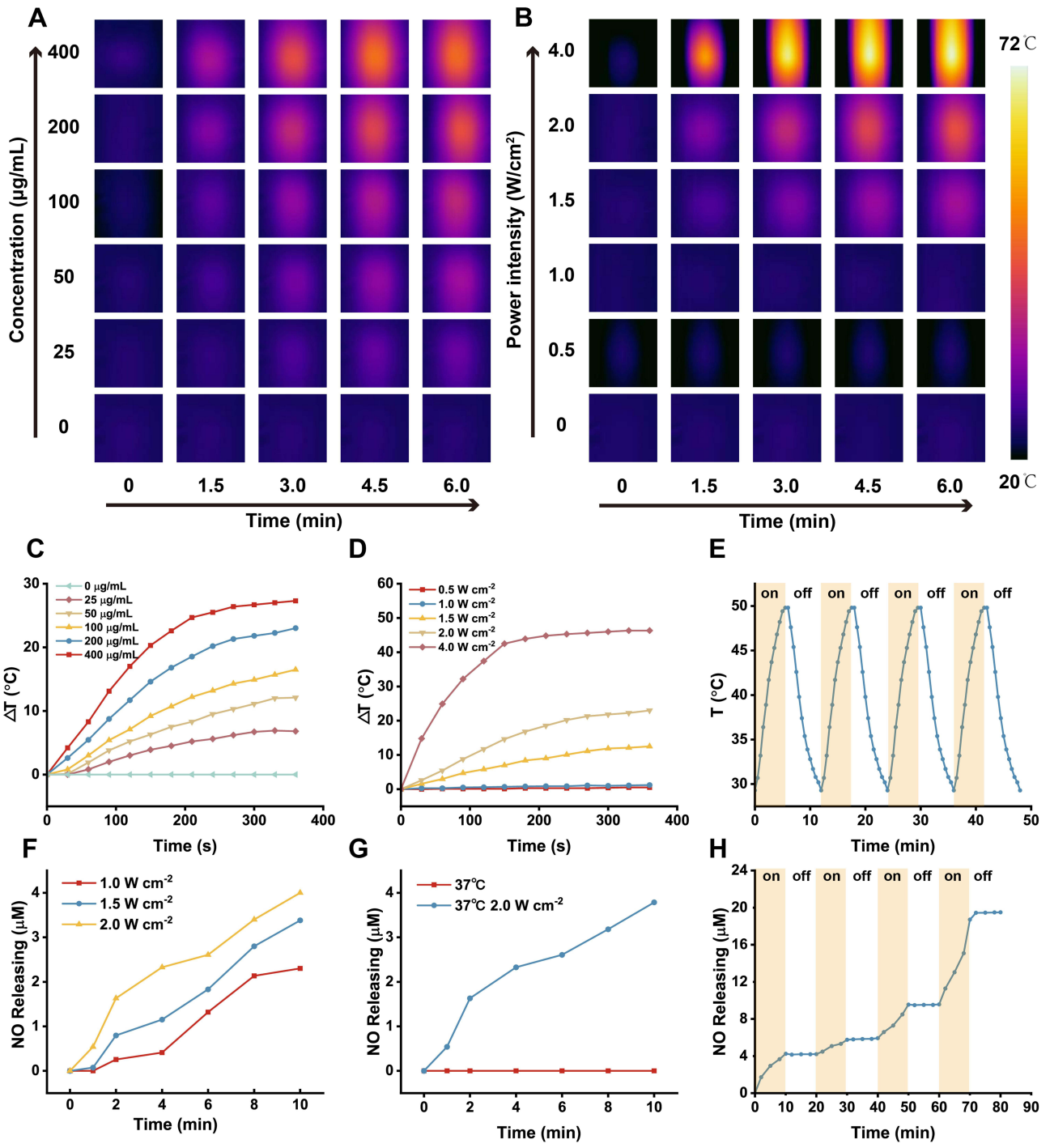

Figure 2 (**A**) Thermal images of GSNPD NPs at elevated concentrations (0, 25, 50, 100, 200, 400 μg/mL) (power density: 2.0 W/cm^2) and (**B**) power densities (0, 0.5, 1.0, 1.5, 2.0, and 4.0 W/cm^2) (concentration: 200 μg/mL). (**C**) Photothermal heating curves at various concentrations of GSNPD NPs (Power density: 2.0 W/cm^2), and (**D**) at different power densities of GSNPD NPs (concentration: 200 μg/mL). (**E**) The photothermal circulation curve of GSNPD NPs over four laser on/off cycles (concentration: 200 μg/mL, power density: 2.0 W/cm^2). (**F**) The released curves of NO gas from GSNPD NPs at different power densities. (**G**) The NO gas-releasing curves of the GSNPD NPs (200 μg/mL) at 37 °C with or without laser irradiation. (**H**) The generation of NO gas in GSNPD NPs suspensions be triggered on-demand by turning on/off the 808 nm laser (concentration: 200 μg/mL, power density: 2.0 W/cm^2).

concentration of GSNPD NPs to 200 μg/mL, and the temperature could reach to 48 °C under a 808 nm laser (2 W/cm^2). Previous studies have shown that, NO concentration in the range of 4 ~ 6 μM, exhibit significant anti-inflammatory ability.[37] Under this condition, the GSNPD NPs solutions could generate ~19 μM of NO gas after continuous irradiation

https://doi.org/10.2147/IJN.S503774

for 40 min, which was enough for the anti-inflammatory role of NO (Figure S4). In summary, the NIR light-triggered GSNPD NPs for NO gas generating could be a promising photothermal initiated NO donor, achieving light-responsive "on-demand" NO release.

Cellular Toxicity Evaluation and Hemolysis Test

The cellular biocompatibility of GSNPD NPs was evaluated to ensure their safety for biomedical applications in vitro. The results of the CCK-8 assay indicated that GSNPD NPs could not cause a substantial reduction in the cell viability below the concentration of 200 μg/mL, which remained above 80% after incubation overnight (Figure S5A).

The consideration of blood compatibility is a critical factor in evaluating nanomaterials for additional biological applications. Therefore, a hemolysis assay was conducted to assess the blood compatibility of GSNPD NPs. As shown in Figure S5B, no apparent hemolysis was observed in the GSNPD-treated samples, and the hemolysis rates remained below 1.7% even at a nanoparticle concentration as high as 200 μg/mL. These results confirmed the excellent blood compatibility of GSNPD NPs for photothermal/anti-inflammatory treatment.

In vitro Targeting Ability of GSNPD NPs to Activated Macrophages

Activated macrophages play a crucial role as pro-inflammatory cells in atherosclerotic plaques, contributing to the initiation and progression of vascular injury. In this study, LPS was used to induce the formation of pro-inflammatory macrophages, and the inflammatory cytokine release of TNF-α and IL-6 in activated cells increased significantly. The activation of macrophages displayed the surface overexpression of class A scavenger receptors (SR-A).[31,38] Thus, the targeting capability of GSNPD NPs towards activated macrophages was assessed by CLSM and flow cytometry. GSNPD and GSNO were labeled with Rh-6G. As shown in Figure 3A, the green fluorescence from GSNPD and GSNO NPs was mainly localized in the cytoplasm. Pre-treatment with LPS and the existence of DS enhanced the fluorescence signal, indicating that GSNPD NPs possessed a higher targeting ability to pro-inflammatory macrophages. Results in flow cytometry and inductively coupled plasma−mass spectrometry (ICP-MS) were highly consistent with the above findings (Figures 3B and S7), further demonstrating that GSNPD NPs were more accessible to the activated macrophages than GSNO. Furthermore, the cellular uptake of GSNPD NPs occurred in a time-dependent manner, with green fluorescence intensity gradually increasing over time (Figure 3C and D). Then, we wonder if such specific binding between DS of GSNPD and SR-A overexpressed in activated RAW264.7 cells could inhibit SR-A mediated uptake of ox-LDL. Thus, after treatment with GSNPD and GSNO NPs, intracellular lipid droplets in macrophages were stained with bright green fluorescence using BODIPY 493/503. As shown in Figure 3E, compared with LPS pre-treated macrophages, GSNPD could significantly reduce the uptake of ox-LDL. In contrast, no noticeable difference was observed between the GSNO and LPS groups in the activated macrophages (Figure 3F), indicating that GSNPD could inhibit the foaming of macrophages to some extent. In conclusion, these data showed that GSNPD NPs owned a macrophage-targeting capability in vitro. SR-A, over-expressed by activated macrophages, was occupied by GSNPD NPs, thereby decreasing endocytosis of ox-LDL. This effect would be beneficial for atherosclerosis treatment.

Combined PTT and Anti-Inflammatory Treatment in vitro

GSNPD NPs have a good photothermal conversion and NO generation ability, which allows us to further validate their role in PTT and anti-inflammatory therapy in vitro. The activated RAW264.7 cells were exposed to various concentrations of GSNPD NPs with or without 808 nm laser irradiation (2.0 W/cm^2, 5 min). As shown in Figure 4A, there was no noticeable decline of cell viability without any laser irradiation for all groups, indicating the good cellular biocompatibility of GSNPD NPs and biosafety of 808 nm laser irradiation. However, after exposure to 808 nm irradiation, cell viability decreased with increasing concentrations of GSNPD NPs. However, the cell survival rate at 200 μg/mL was only 31.39% in the laser group, indicating that the photothermal ablation effect of GSNPD NPs could effectively inhibit the proliferation of macrophages. It should be pointed that the cytotoxicity of GSNPD + laser on normal macrophages was also assessed, and the results demonstrated that only relatively low toxicity to normal macrophages was observed (Figure S8). Then, we systematically compared the PTT effects after different treatments (GSNO, GSNPD, GSNO + laser, and GSNPD + laser) by cell viability experiment, live/dead co-staining and apoptosis assessment. The cell

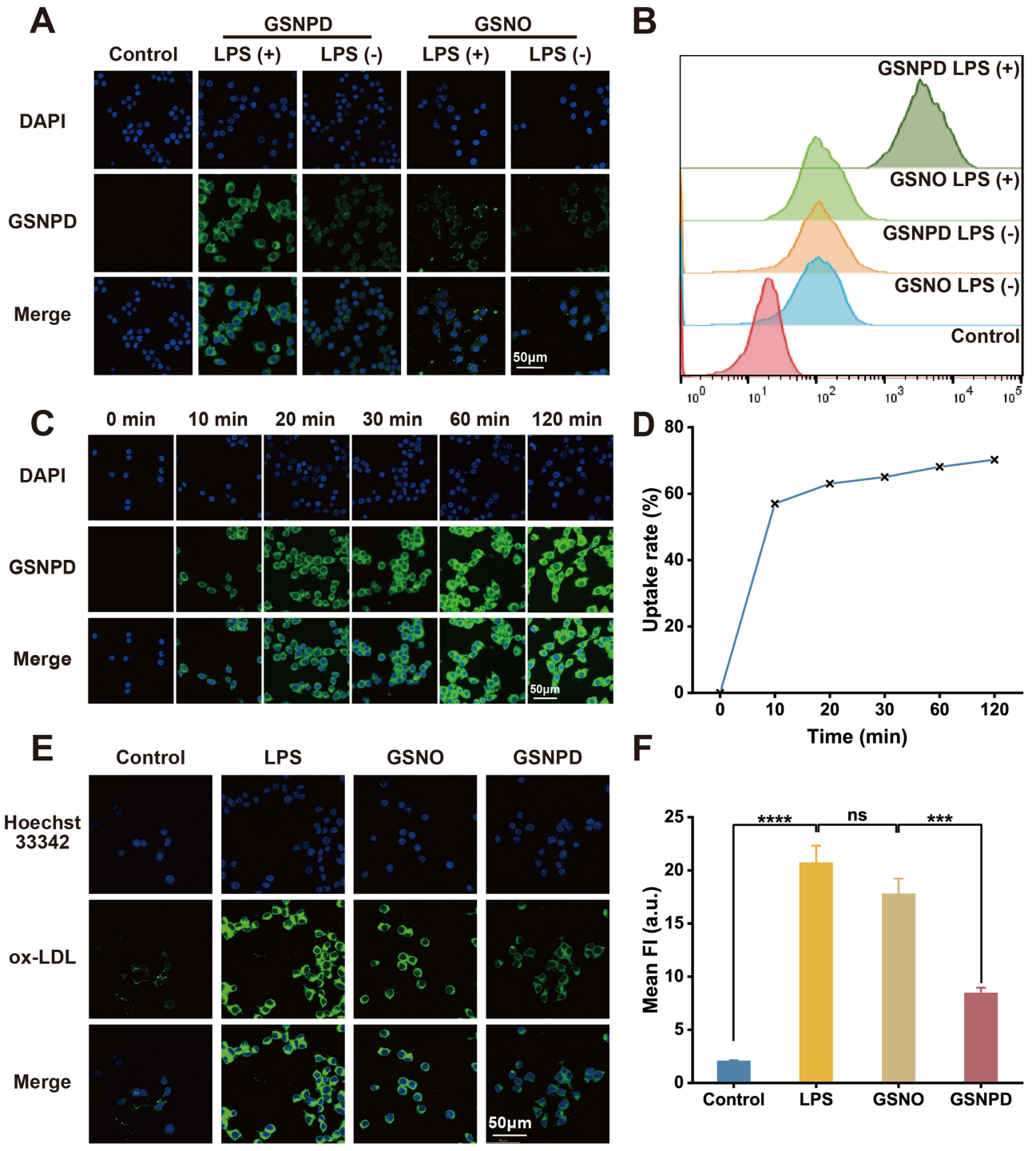

Figure 3 (**A**) The CLSM images of RAW 264.7 cells and LPS activated RAW264.7 cell incubated with GSNO NPs or GSNPD NPs for 30 min. Scale bar: 50 μm. (**B**) Flow cytometric analysis of the intracellular fluorescence intensity of cells with different treatments. (**C**) The CLSM images of activated RAW264.7 cells treated with GSNPD NPs at different time points. Scale bar: 50 μm. (**D**) Half-quantitative analysis of the GSNPD NPs uptake in RAW264.7 cells at different time points. (**E**) Representative confocal fluorescence images of macrophages after different pre-treatments (control, LPS, GSNO, or GSNPD NPs) and then incubated with ox-LDL. (**F**) Fluorescence intensity analysis of the fluorescent intensity in (**E**) (n = 3) (***P < 0.001, ****P < 0.0001).
Abbreviations: ns, no significance.

viabilities in laser only, GSNO and GSNPD group, were 99.54%, 92.49% and 89.02%, respectively, which were reduced to 65.3% for GSNO + laser group and 31.39% for GSNPD + laser group (Figure 4B), displaying the excellent photothermal ablation effect of GSNPD NPs on activated macrophages. To visually observe such performance, the live/dead co-staining was performed. As shown in Figure 4C, cells were double stained with Calcein-AM (green) and PI

https://doi.org/10.2147/IJN.S503774

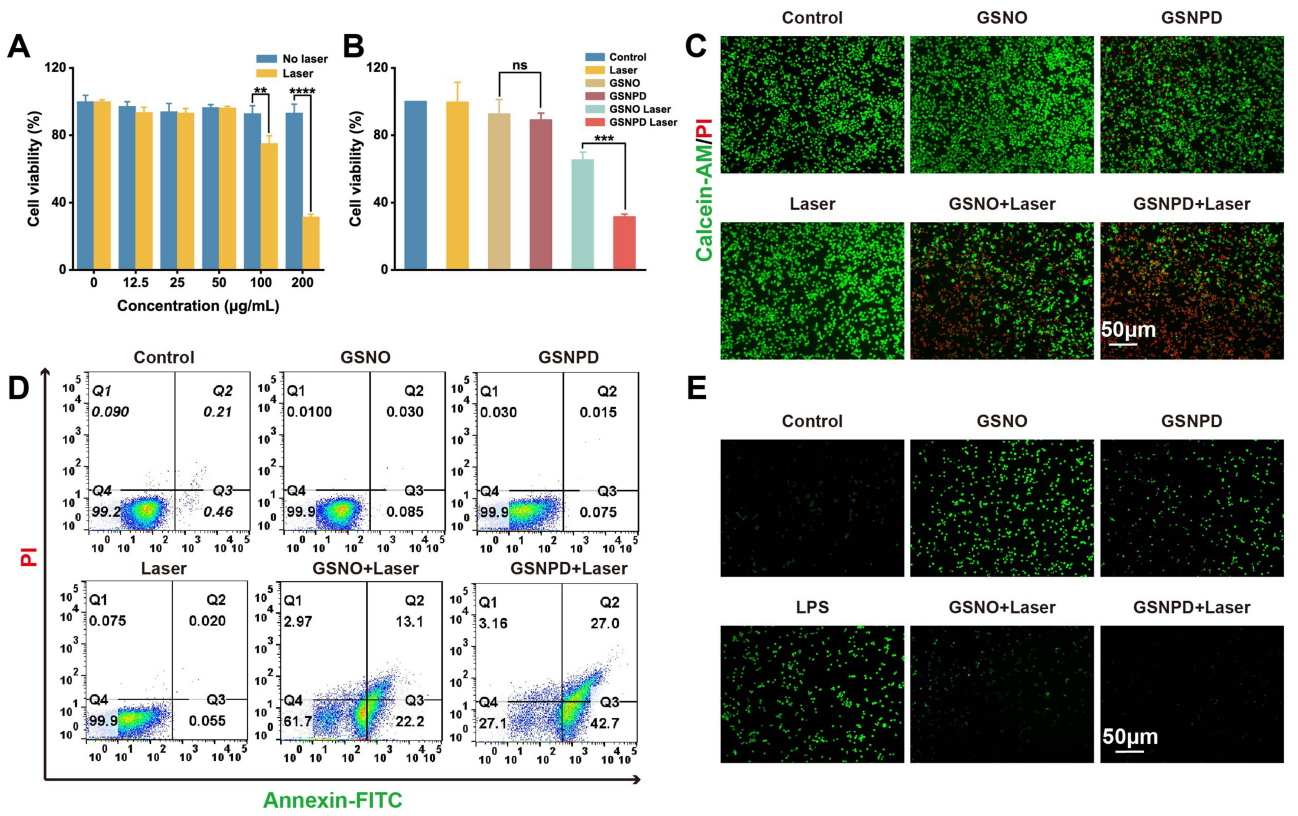

Figure 4 (**A**) Cell viabilities of activated RAW264.7 cells incubated with GSNPD NPs at various concentrations with or without laser (power density: 2.0 W/cm^2, 5 min) (n = 3) (**P < 0.01, ****P < 0.0001). (**B**) Cell viability assessment of RAW264.7 following different treatments (n = 3) (***P < 0.001, ns: no significance). (**C**) Fluorescent signal images of live/dead co-stained macrophages after various treatments. (**D**) Flow cytometric assessment of apoptotic macrophages following different interventions. (**E**) Fluorescence images depicted the intracellular generation of ROS after various treatments. Scale bar: 50 μm.

(red). Consistent with the cell viability results, several dead cells were observed in the GSNO + laser (2 W/cm^2, 5 min) group, which further increased in the GSNPD + laser (2 W/cm^2, 5 min) group. The cells were stained with Annexin V-FITC/PI to evaluate cell apoptosis and necrosis following various treatments by flow cytometry (Figure 4D). As expected, GSNPD + laser (2 W/cm^2, 5 min) induced the highest level of apoptotic cell death amidst all other groups. The high apoptotic rate of up to ~70% demonstrated that GSNPD + laser (2 W/cm^2, 5 min) was an advanced method for inducing macrophage apoptosis. Overexpression of ROS in pro-inflammatory macrophages within atherosclerosis plaques promotes the secretion of pro-inflammatory cytokines, which contributes to the plaque progression by sustaining a persistent inflammatory microenvironment.[39] It is expected that the ablation of inflammatory macrophages will reduce the generation of ROS. In light of this knowledge, we assessed the ability of GSNPD NPs to inhibit the generation of ROS in macrophages. As expected, compared with the control group, RAW264.7 cells generated higher ROS after LPS treatment (Figure 4E, control and model group). By contrast, a faint green fluorescence was observed after treatment with GSNO + laser or GSNPD + laser and the weakest signal was displayed in the GSNPD + laser group, demonstrating significant ROS generation inhibition was realized. This result may be the combined effect of photothermal ablation of inflammatory macrophages and NO anti-inflammation to improve the micro-environment. Additionally, GSNPD + laser treatment on normal macrophages resulted in negligible ROS production, further illustrating the weak influence of our strategy on normal macrophages (Figure S9).

Inflammation Inhibition Performance of GSNPD NPs

The progression of atherosclerosis is linked to chronic inflammation. The reported study constructed a platelet-mimicking nano-prodrug system, which utilized the photo-controlled release of NO. NO could transform the atherosclerotic plaque micro-environment from pro-inflammatory to anti-inflammatory, inhibiting the progression of atherosclerotic plaques.[21]

To further investigate the progression of atherosclerosis by reshaping the plaque micro-environment after photothermal ablation, we first detected pro-inflammatory cytokines secreted by activated inflammatory macrophages (LPS-treated) by ELISA analysis. The inflammatory cytokines (TNF-α and IL-6) secreted by RAW264.7 cells significantly elevated after LPS stimulation (Figure S6). The comparison among LPS, laser and GSPD + laser groups showed that PTT ablation of activated macrophages resulted in increased production of pro-inflammatory cytokines (Figure 5A and B). However, in the GSNO + laser (2 W/cm^2, 5 min) group, the levels of pro-inflammatory cytokines were significantly lowered compared to the GSPD + laser (2 W/cm^2, 5 min) group, suggesting that this reduction may be attributed to NO generation. Additionally, the GSNPD + laser (2 W/cm^2, 5 min) group exhibited a more substantial inhibition of inflammatory factors, likely due to the synergistic effect of the targeting molecule DS and the released NO.

Inhibition of Foam Cell Formation

Some inflammatory factors are reported to promote macrophage foaming. The ability of inflammatory cytokines to induce cholesterol accumulation in macrophage cells can explain the relationship between lipidosis and inflammation in the progress of atherosclerotic lesions.[40,41] The above results indicated that treatment with GSNO + laser and GSNPD + laser significantly reduced the release of inflammatory cytokines from activated macrophages. Therefore, we evaluated whether such changes in the microenvironment would inhibit macrophage foaming. We placed untreated RAW264.7 cells

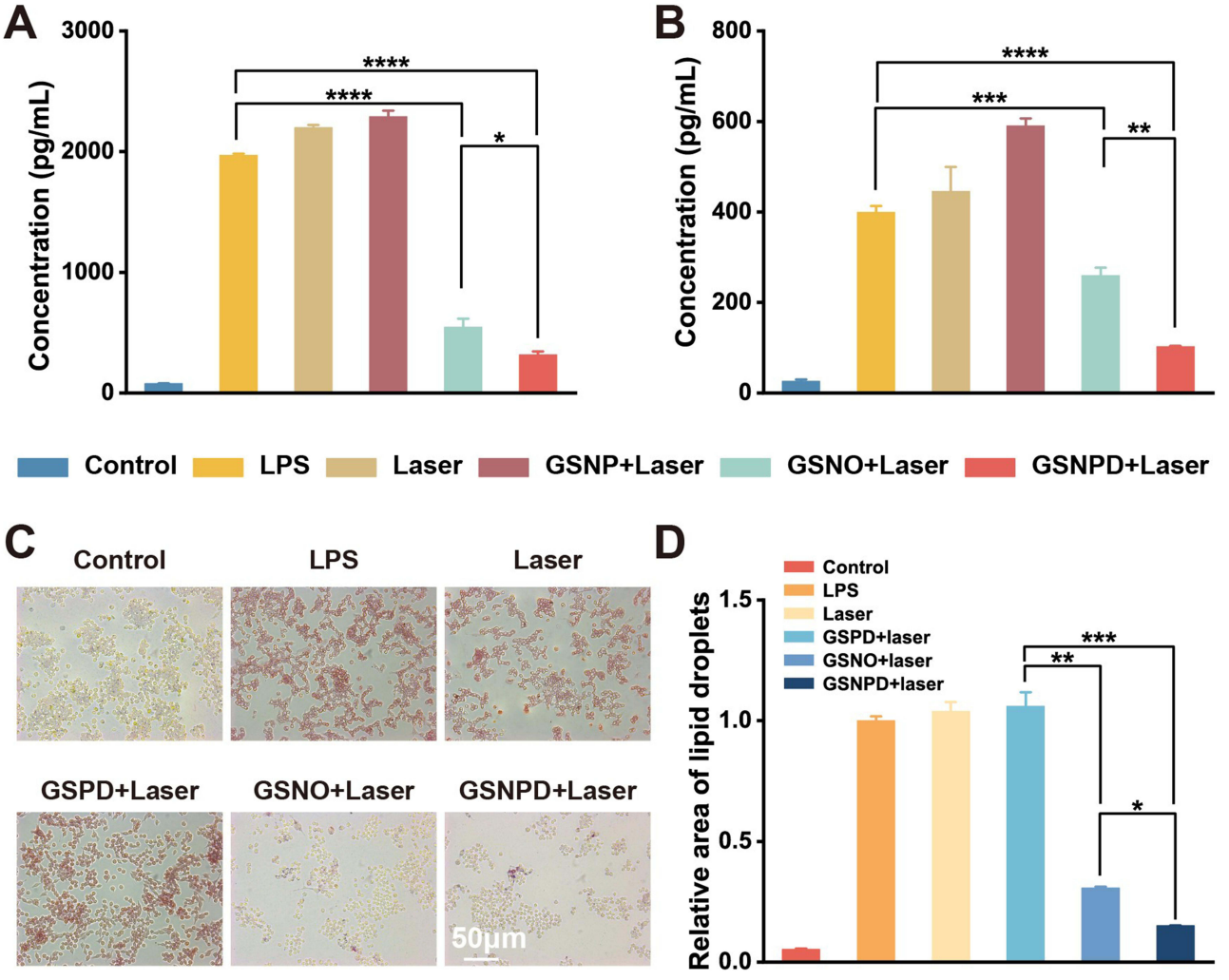

Figure 5 Secretion of typical pro-inflammatory factors (**A**) TNF-α and (**B**) IL-6 by RAW264.7 cells after different treatments (n = 3) (*P < 0.05, **P < 0.01, ***P < 0.001, ****P < 0.0001). (**C-D**) Optical microscopy images showing foam cell formation induced by oxLDL in macrophages, along with semi-quantitative analysis (n = 3) (*P < 0.05, **P < 0.01, ***P < 0.001).

https://doi.org/10.2147/IJN.S503774

in the bottom chamber and inoculated RAW264.7 cells that had undergo different treatments in the upper chamber. The degree of macrophage foaming was assessed using Oil Red O (ORO) staining. As shown in Figure 5C and D, a substantial number of foam cells were observed in the bottom chamber following LPS, laser, and GSPD + laser treatments in the upper chamber. However, when the cells in the upper chamber were treated with GSNO + Laser or GSNPD + Laser, fewer foam cells were observed in the bottom chamber, indicating that the improved micro-environment by GSNPD + laser could inhibit the progression of atherosclerosis.

Discussion

In brief, this study developed multifunctional nanoparticles, GSNPD for exploring the synergistic anti-atherosclerotic effects of PTT and anti-inflammation. In the near-infrared (NIR) I region, GSNPD NPs displayed intense absorption, endowing them with excellent photothermal conversion property. Meanwhile, heat-sensitive S-nitrosothiols (RSNO) molecules for the on-demand release of the anti-inflammatory nitric oxide (NO) were loaded on Au NR@SiO_2 through covalent conjugation. By disrupting the S-NO bonding of RSNO, the NIR laser could trigger the controlled NO generation for inflammation inhibition. Additionally, by further modifying dextran sulfate (DS), GSNPD could exhibit the potential to selectively target scavenger receptor A (SR-A) overexpressed on the surface of pro-inflammatory macrophages within plaques. By integrating PTT with anti-inflammatory mechanisms through laser-activated NO release, GSNPD offers a dual-pronged attack on the disease. Photothermal therapy effectively ablates inflammatory macrophages, while thermally triggered GSNPD NPs facilitate the release of NO. Under irradiation at an intensity of 2 W/cm², the ablated inflammatory macrophages cease to produce inflammatory factors and ROS. The NO of micro-environment exerts anti-inflammatory and antioxidant effects, thereby enhancing endothelial cell function and contributing synergistically to the improvement of the inflammatory micro-environment. The synergistic effect of photothermal ablation of inflammatory macrophages and NO anti-inflammation can effectively inhibit ROS in the inflammatory micro-environment. The experimental results of our existing in vitro have suggested that the fabricated GSNPD NPs have positive effects on anti-atherosclerosis by pro-inflammatory macrophages ablation, NO production and ROS scavenging, providing a feasible approach for PTT-based atherosclerosis therapy. However, we have to point out that further in vivo studies should be carried out to comprehensively evaluate their therapeutic efficacy under the complex interplay between the various components of the atherosclerotic plaque and the immune system as well as a deeper understanding of how GSNPD interacts with these systems in vivo.

Conclusion

In conclusion, this study has developed multifunctional nanoparticles, GSNPD for exploring the synergistic anti-atherosclerotic effects of PTT and anti-inflammation. It can effectively and accurately ablate pro-inflammatory macrophages by recognizing and targeting to SR-A overexpressed the activated macrophages of arterial plaques, and simultaneously inhibit PTT-induced inflammation through the laser-activated NO release in situ, which provided a new idea for PTT-based AS treatment.

Data Sharing Statement

The data that has been used is confidential.

Acknowledgments

This work was supported by the Natural Science Foundation of Jiangsu Province (BK20221391), Pengcheng Talent-Medical Key Talent Training Project, Innovation and Entrepreneurship Training Program for College Students in Jiangsu Province (202210313021Z).

Author Contributions

All authors made a significant contribution to the work reported, whether that is in the conception, study design, execution, acquisition of data, analysis and interpretation, or in all these areas; took part in drafting, revising or critically reviewing the article; gave final approval of the version to be published; have agreed on the journal to which the article has been submitted; and agree to be accountable for all aspects of the work.

Disclosure

The authors declare no financial conflict of interest.

References

1. Galkina E, Ley K. Immune and inflammatory mechanisms of atherosclerosis. *Annu Rev Immunol*. 2009;27(1):165–197. doi:10.1146/annurev.immunol.021908.132620
2. Prabhakaran D, Jeemon P, Roy A. Cardiovascular diseases in India. *Circulation*. 2016;133(16):1605–1620. doi:10.1161/CIRCULATIONAHA.114.008729
3. Herrington W, Lacey B, Sherliker P, Armitage J, Lewington S. Epidemiology of atherosclerosis and the potential to reduce the global burden of atherothrombotic disease. *Circ Res*. 2016;118(4):535–546. doi:10.1161/CIRCRESAHA.115.307611
4. Chong SY, Wang X, van Bloois L, et al. Injectable liposomal docosahexaenoic acid alleviates atherosclerosis progression and enhances plaque stability. *J Control Release*. 2023;360:344–364. doi:10.1016/j.jconrel.2023.06.035
5. Yanagawa T, Shibata A, Tabata S, Kurita E, Ikeda S, Ikeda T. Case of effective suction to secure the true lumen for acute occlusion after carotid endarterectomy. *Radiol Case Rep*. 2022;17(11):4144–4147. doi:10.1016/j.radcr.2022.08.008
6. Budoff MJ, Ellenberg SS, Lewis CE, et al. Testosterone treatment and coronary artery plaque volume in older men with low testosterone. *JAMA*. 2017;317(7):708–716
7. Nicholls SJ, Ballantyne CM, Barter PJ, et al. Effect of two intensive statin regimens on progression of coronary disease. *N Engl J Med*. 2011;365(22):2078–2087. doi:10.1056/NEJMoa1110874
8. Vazquez-Prada KX, Moonshi SS, Xu ZP, Ta HT. Photothermal nanomaterials for theranostics of atherosclerosis and thrombosis. *Appl Mater Today*. 2023;35:16.
9. Nomura S, Morimoto Y, Tsujimoto H, et al. Highly reliable, targeted photothermal cancer therapy combined with thermal dosimetry using a near-infrared absorbent. *Sci Rep*. 2020;10(1):9765. doi:10.1038/s41598-020-66646-x
10. Liu J, Smith S, Wang C. Reversing the epithelial-mesenchymal transition in metastatic cancer cells using CD146-targeted black phosphorus nanosheets and a mild photothermal treatment. *ACS Nano*. 2022;16(2):3208–3220. doi:10.1021/acsnano.1c11070
11. Liu S, Zhao Y, Shen M, et al. Hyaluronic acid targeted and pH-responsive multifunctional nanoparticles for chemo-photothermal synergistic therapy of atherosclerosis. *J Mat Chem B*. 2022;10(4):562–570. doi:10.1039/D1TB02000E
12. Dai T, He W, Yao C, et al. Applications of inorganic nanoparticles in the diagnosis and therapy of atherosclerosis. *Biomater Sci*. 2020;8(14):3784–3799. doi:10.1039/D0BM00196A
13. Pan W, Cheng J, Cao X, et al. Niobium carbide MXenzyme-Driven comprehensive cholesterol regulation for photoacoustic image-guided and anti-inflammatory photothermal ablation in atherosclerosis. *Bioact Mater*. 2024;36:565–579. doi:10.1016/j.bioactmat.2024.07.001
14. Mao J, Wu C, Zheng L, et al. Advances in stimulus-responsive nanomedicine for treatment and diagnosis of atherosclerosis. *Colloids Surf B Biointerfaces*. 2025;245:114298. doi:10.1016/j.colsurfb.2024.114298
15. Liu Y, Bhattarai P, Dai Z, Chen X. Photothermal therapy and photoacoustic imaging via nanotheranostics in fighting cancer. *Chem Soc Rev*. 2019;48(7):2053–2108. doi:10.1039/c8cs00618k
16. Liu T, Li X, Wang J, et al. Ag@S-nitrosothiol core–shell nanoparticles for chemo and photothermal synergistic tumor targeted therapy. *J Mat Chem B*. 2020;8(25):5483–5490. doi:10.1039/D0TB00734J
17. Lu R, Zhu J, Yu C, Nie Z, Gao Y. Cu(3)BiS(3) nanocrystals as efficient nanoplatforms for CT imaging guided photothermal therapy of arterial inflammation. *Front Bioeng Biotechnol*. 2020;8:981. doi:10.3389/fbioe.2020.00981
18. Zhang X, Liu J, Yang X, et al. CuCo2S4 nanocrystals as a nanoplatform for photothermal therapy of arterial inflammation. *Nanoscale*. 2019;11(19):9733–9742. doi:10.1039/C9NR00772E
19. Liu XM, Shan GS, Yu JS, et al. Laser heating of metallic nanoparticles for photothermal ablation applications. *AIP Adv*. 2017;7(2):025308–12.
20. Parks BW, Phimister EG, Lusis AJ. Macrophage accumulation in atherosclerosis. *N Engl J Med*. 2013;369(24):2352–2353. doi:10.1056/NEJMcibr1312709
21. Robbins CS, Hilgendorf I, Weber GF, et al. Local proliferation dominates lesional macrophage accumulation in atherosclerosis. *Nat Med*. 2013;19(9):1166–1172. doi:10.1038/nm.3258
22. Suzuki H, Kurihara Y, Takeya M, et al. A role for macrophage scavenger receptors in atherosclerosis and susceptibility to infection. *Nature*. 1997;386(6622):292–296. doi:10.1038/386292a0
23. Chen W, Schilperoort M, Cao Y, Shi J, Tabas I, Tao W. Macrophage-targeted nanomedicine for the diagnosis and treatment of atherosclerosis. *Nat Rev Cardiol*. 2021;19(4):228–249. doi:10.1038/s41569-021-00629-x
24. Cao Z, Yuan G, Zeng L, et al. Macrophage-targeted sonodynamic/photothermal synergistic therapy for preventing atherosclerotic plaque progression using CuS/TiO2 heterostructured nanosheets. *ACS Nano*. 2022;16(7):10608–10622. doi:10.1021/acsnano.2c02177
25. Yang M, Ding J, Feng X, et al. Scavenger receptor-mediated targeted treatment of collagen-induced arthritis by dextran sulfate-methotrexate prodrug. *Theranostics*. 2017;7(1):97–105. doi:10.7150/thno.16844
26. Herman AG, Moncada S. Therapeutic potential of nitric oxide donors in the prevention and treatment of atherosclerosis. *Eur Heart J*. 2005;26(19):1945–1955. doi:10.1093/eurheartj/ehi333
27. Loscalzo J. Nitric oxide signaling and atherothrombosis redux. *Circulation*. 2018;137(3):233–236. doi:10.1161/CIRCULATIONAHA.117.032901
28. Chai Y, Shangguan L, Yu H, et al. Near infrared light-activatable platelet-mimicking NIR-II NO nano-prodrug for precise atherosclerosis theranostics. *Adv Sci*. 2023;11(3):2304994.
29. Zhao Y, Jiang C, He J, et al. Multifunctional dextran sulfate-coated reconstituted high density lipoproteins target macrophages and promote beneficial antiatherosclerotic mechanisms. *Bioconjug Chem*. 2017;28(2):438–448. doi:10.1021/acs.bioconjchem.6b00600
30. Ye M, Zhou J, Zhong Y, et al. SR-A-targeted phase-transition nanoparticles for the detection and treatment of atherosclerotic vulnerable plaques. *ACS Appl Mater Interfaces*. 2019;11(10):9702–9715. doi:10.1021/acsami.8b18190
31. You DG, Saravanakumar G, Son S, et al. Dextran sulfate-coated superparamagnetic iron oxide nanoparticles as a contrast agent for atherosclerosis imaging. *Carbohydr Polym*. 2014;101:1225–1233. doi:10.1016/j.carbpol.2013.10.068

32. Jia Q, Ge J, Liu W, et al. Gold nanorod@silica-carbon dots as multifunctional phototheranostics for fluorescence and photoacoustic imaging-guided synergistic photodynamic/photothermal therapy. *Nanoscale*. 2016;8(26):13067–13077. doi:10.1039/C6NR03459D
33. Liu J, Zhou B, Guo Y, et al. SR-A-targeted nanoplatform for sequential photothermal/photodynamic ablation of activated macrophages to alleviate atherosclerosis. *ACS Appl Mater Interfaces*. 2021;13(25):29349–29362. doi:10.1021/acsami.1c06380
34. Chen Y-S, Frey W, Kim S, Kruizinga P, Homan K, Emelianov S. Silica-coated gold nanorods as photoacoustic signal nanoamplifiers. *Nano Lett*. 2011;11(2):348–354. doi:10.1021/nl1042006
35. Liu P, Wang Y, Liu Y, Tan F, Li J, Li N. S-nitrosothiols loaded mini-sized Au@silica nanorod elicits collagen depletion and mitochondrial damage in solid tumor treatment. *Theranostics*. 2020;10(15):6774–6789. doi:10.7150/thno.42661
36. Ganzarolli de Oliveira M. S-nitrosothiols as platforms for topical nitric oxide delivery. *Basic Clin Pharmacol Toxicol*. 2016;119(S3):49–56. doi:10.1111/bcpt.12588
37. Wang S, Wang Y, Lai X, et al. Minimalist nanocomplex with dual regulation of endothelial function and inflammation for targeted therapy of inflammatory vascular diseases. *ACS Nano*. 2023;17(3):2761–2781. doi:10.1021/acsnano.2c11058
38. de Winther MP, van Dijk KW, Havekes LM, Hofker MH. Macrophage scavenger receptor class A: a multifunctional receptor in atherosclerosis. *Arterioscler Thromb Vasc Biol*. 2000;20(2):290–297. doi:10.1161/01.ATV.20.2.290
39. Yang Q, Jiang H, Wang Y, et al. Plaque macrophage-targeting nanosystems with cooperative Co-regulation of ROS and TRAF6 for stabilization of atherosclerotic plaques. *Adv Funct Mater*. 2023;33(28):2301053. doi:10.1002/adfm.202301053
40. McLaren JE, Michael DR, Ashlin TG, Ramji DP. Cytokines, macrophage lipid metabolism and foam cells: implications for cardiovascular disease therapy. *Prog Lipid Res*. 2011;50(4):331–347. doi:10.1016/j.plipres.2011.04.002
41. Orekhov AN, Markin AM, Sukhorukov VN, Khotina VA, Ivanova E. Pro-inflammatory molecules induce cholesterol accumulation in macrophages: role of inflammatory response in foam cell formation. *Atherosclerosis*. 2021;320:129–130. doi:10.1016/j.atherosclerosis.2021.01.007